THE ASTROPHYSICAL JOURNAL, 247: 879–893, 1981 August 1

SUPERNOVA REMNANTS IN M31

WILLIAM P. BLAIR AND ROBERT P. KIRSHNER[1,2]
Department of Astronomy, University of Michigan
AND
ROGER A. CHEVALIER[1]
Department of Astronomy, University of Virginia
Received 1980 November 18; accepted 1981 February 11

ABSTRACT

Image-tube photographs of eight fields in M31, using interference filters that isolate Hα + [N II] and [S II], have revealed nebulae that may be supernova remnants in this galaxy. Spectroscopic observations show that 11 of these nebulae resemble galactic supernova remnants (SNRs). The [O III] temperatures determined for four of these SNRs are in the range of 37,000–65,000 K. The [S II] ratios indicate densities in the S^+ zone in the range of 150–730 cm^{-3}. An estimate of the pressure in the optical filaments and the measured diameter permit an estimate of the initial energy in each remnant; we find a mean value of $E_0 \approx 3 \times 10^{50}$ ergs. However, the energy calculated in this way appears to be correlated with the remnant's diameter, an effect which may be related to magnetic pressure in the filaments. Interpretation of the remnant spectra through shock-wave models suggests an increase in the nitrogen abundance by a factor of 4 from the outermost SNR near 20 kpc to the innermost near 4 kpc. Some of these SNRs might be detectable as radio sources with the Very Large Array (VLA) telescope; two of them are coincident with *Einstein* X-ray sources.

Subject headings: galaxies: individual — nebulae: abundances — nebulae: supernova remnants

I. INTRODUCTION

The study of extragalactic supernova remnants (SNRs) has just begun, with remnants detected in the Magellanic Clouds (Mathewson and Clarke 1972) and in M33 (D'Odorico, Benvenuti, and Sabbadin 1978). Extragalactic remnants provide a set of objects in which the angular diameter corresponds to the linear size, which makes the study of remnant evolution much easier than in our own Galaxy. In addition, the expanding shock wave of a supernova remnant heats the interstellar gas of a galaxy: the optical line emission emitted by the gas as it cools can be used to estimate chemical abundances in galaxies over a large range in galactocentric distance. In this work, we discuss the detection of SNRs in M31 by optical means, present spectrophotometry of 15 objects (11 of which we believe to be SNRs), discuss the energetics of the remnants, and present evidence for an abundance gradient in M31.

Galactic supernova remnants have been identified by both radio surveys and optical searches. Radio surveys (Clark and Caswell 1976 and references therein) have revealed about 125 nonthermal extended sources. Because of galactic obscuration, only about 29 have been detected optically with broad-band plates in systematic surveys (van den Bergh 1978; van den Bergh, Marscher, and Terzian 1973), although interference filter photographs (Blair *et al.* 1980) and plates with large telescopes (Kirshner and Winkler 1979) have added a few individual objects.

The first systematic attempt to identify extragalactic SNRs was the pioneering work of Mathewson and Clarke (1972; 1973*a*, *b*) on the Magellanic Clouds. Their approach was to identify shock-heated nebulae through interference filter photographs and to combine these data with radio surveys of the Clouds that served to identify nonthermal sources. In particular, they used image-tube plates taken through filters that isolated the emission lines of Hα + [N II] at λ6570 and the [S II] lines at λ6725. In galactic SNRs, and shock-heated nebulae generally, the ratio $I(\text{H}\alpha + [\text{N II}])/I([\text{S II}])$ is typically less than 2, while in photoionized nebulae it is generally considerably larger. Mathewson and Clarke also surveyed the Clouds at 408 MHz and used their data along with previous radio surveys to determine which sources had nonthermal spectra. In all, 12 SNRs were found in the Large Magellanic Cloud (LMC) and two were identified in the Small Magellanic Cloud (SMC).

Although radio surveys are effective in detecting SNRs in our Galaxy and in the Magellanic Clouds, the spatial resolution and sensitivity of radio surveys has limited their effectiveness in detecting more distant SNRs. For example, for M33, Israel and van der Kruit (1974) obtained 21 cm observations with a resolution of 23″ × 45″ (75 × 158 pc) and a 2σ limit in flux density of 1.2 mJy. For comparison, at the distance of M33 (assuming 720 kpc) the Cygnus Loop would have a flux density of 0.3 mJy and a diameter of about 9″.

In M33, the optical method for finding SNRs has been very successful. Interference filter photographs of M33

[1] Guest Observer, Kitt Peak National Observatory, operated by the Association of Universities for Research in Astronomy, Inc., under contract with the National Science Foundation.
[2] Alfred P. Sloan Research Fellow.

have been obtained by D'Odorico, Benvenuti, and Sabbadin (1978), Sabbadin (1978), and Sabbadin and Bianchini (1979), and a total of 19 SNR candidates have been identified. About half of these objects coincide with radio sources from Israel and van der Kruit's (1974) 21 cm map, but the balance were identified as SNR candidates only by their appearance on interference filter photographs. Twelve of these objects have now been confirmed as SNRs by optical spectrophotometry (Danziger *et al.* 1979; Dopita, D'Odorico, and Benvenuti 1980). In addition, radio maps obtained at the Very Large Array (VLA) telescope by Goss *et al.* (1980) have now confirmed the nonthermal nature of the radio spectra for three of the four objects observed by Danziger *et al.* (1979).

We have investigated M31, which is a slightly more difficult case than M33 because of its angular extent and small inclination to the line of sight ($\sim 13°$). The first information on possible SNRs in M31 came from the study of M31 kinematics. Based on image-tube spectra of 53 emission-line regions, Rubin, Kumar, and Ford (1972, hereafter RKF) found seven objects with peculiar spectra. Kumar (1976) concluded that they were SNRs.

Recently, D'Odorico, Dopita, and Benvenuti (1980, hereafter DDB1) have surveyed a number of nearby galaxies for SNRs based on interference-filter photographs. Their list for M31, based on $I(\mathrm{H}\alpha + [\mathrm{N\ II}])/([\mathrm{S\ II}])$, contains 19 candidates, including the 7 discussed by Kumar (1976). Independently, we have obtained interference-filter photographs of M31 and have identified many of the same SNR candidates as DDB1, with a few notable exceptions that are discussed in § II. Comparing these two independent searches provides some information regarding the accuracy and the limitations of this technique for discovering SNRs.

We have obtained spectrophotometry of 15 of the SNR candidates, and we find that 11 of them are spectroscopically confirmed as remnants. The spectra, which are presented in § II, are adequate to derive the pressure in each remnant and to provide a rough classification of the shock velocity. In § III we derive the initial energy for each remnant.

The spectra can also be used to investigate, at least qualitatively, the presence of a gradient in interstellar abundances in M31. The remnants span the range from 4 to 20 kpc in galactocentric distance. The interpretation of the SNR spectra in terms of abundances is made possible by the shock models computed by Dopita (1977*a*), Raymond (1979), and Shull and McKee (1979). As we demonstrate in § III, the use of SNRs to determine abundances is not trouble free, but it involves a different set of difficulties from those encountered using H II regions. Also in § III, we compare our results for M31 with the investigation of M33 SNRs by Dopita, D'Odorico, and Benvenuti (1980, hereafter DDB2). In § IV we predict the radio and X-ray properties of the remnants we have studied.

II. OBSERVATIONS

a) Image-Tube Photography

To obtain interference filter plates of M31, we have mounted a 144 mm image tube at the $f/7.5$ focus of the 1.3 m telescope of the McGraw-Hill Observatory. The image tube, on loan from Kitt Peak National Observatory (KPNO) is a single-stage ITT tube with an extended S-20 photocathode, magnetic focussing, and a fiber optic output. The image tube is cooled to 5° C by circulating cold methanol and dried by a flow of desiccated nitrogen.

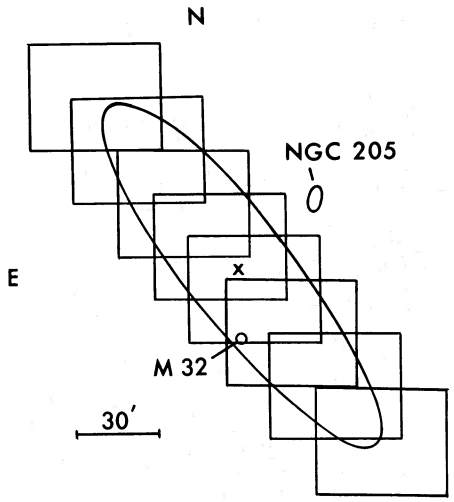

FIG. 1.—Approximate positions of the eight fields photographed in Hα + [N II], [S II], and continuum filter. The large ellipse approximately represent the visible emission on the red POSS plate for M31. NGC 205 and M32 are also indicated.

At $f/7.5$, the original plate scale is 22″ mm^{-1}, and the useful field, which is limited by the telescope's coma, is about 30′ in diameter. We have obtained plates in eight overlapping fields extending about 100′ NE and SW from the galaxy nucleus, as illustrated in Figure 1. Each field was photographed using filters at Hα + [N II], [S II], and in the red continuum to discriminate foreground stars from small, bright emission regions. The interference filters are those used by Parker, Gull, and Kirshner (1979) in their emission-line survey of the Milky Way. Details of the filters are given in Table 1.

All the plates were taken on 4″ × 5″ IIa-D plates, baked 1 hour at 65° C in forming gas (2% hydrogen, 98% nitrogen), and developed for 5 minutes in D-19. For the Hα + [N II] and [S II] plates, exposures were between 2 and 3 hours, as detailed in Table 2. We have compared the Hα + [N II] images with the [S II] images on all the plates, using the blink comparator at Case Western Reserve

TABLE 1

144 mm IMAGE-TUBE FILTER INFORMATION

Filter	λ central (Å)	FWHM (Å)	Peak Transmission (%)
Hα + [N II]	6570	75	56
[S II]	6736	50	67
KP No. 814 (continuum)	6915	114	...
RG 695	(Broad-band Red Continuum)		

TABLE 2

M31 IMAGE-TUBE PHOTOGRAPHS

Field Center	Filter	Date (UT)	Exposure (minutes)
80′ NE	Hα + [N II]	1979 Oct 15	120
80′ NE	[S II]	1979 Oct 16	150
80′ NE	RG 695	1979 Nov 14	10
55′ NE	Hα + [N II]	1979 Oct 13	130
55′ NE	[S II]	1979 Oct 12	150
55′ NE	RG 695	1979 Nov 14	10
30′ NE	Hα + [N II]	1979 Oct 13	125
30′ NE	[S II]	1979 Oct 15	150
30′ NE	KP No. 814	1979 Oct 16	70
10′ NE	Hα + [N II]	1979 Oct 13	120
10′ NE	[S II]	1979 Oct 14	150
10′ NE	KP No. 814	1979 Oct 16	70
10′ SW	Hα + [N II]	1979 Jul 6	120
10′ SW	[S II]	1979 Jul 5	130
10′ SW	KP No. 814	1979 Nov 12	70
30′ SW	Hα + [N II]	1979 Nov 10	140
30′ SW	[S II]	1979 Nov 12	130
30′ SW	KP No. 814	1979 Nov 12	70
55′ SW	Hα + [N II]	1979 Nov 10	120
55′ SW	[S II]	1979 Nov 14	120
55′ SW	KP No. 814	1979 Nov 11	70
80′ SW	Hα + [N II]	1979 Nov 11	125
80′ SW	[S II]	1979 Nov 11	125
80′ SW	KP No. 814	1979 Nov 11	80

University, and have identified the emission nebulae which appear to have strong [S II] emission, as listed in Table 3. Figure 2 (Plate 28) shows portions of the photographs centered 10′ NE of the nucleus with several of the SNR candidates marked. We have used the catalogs of H II regions by Baade and Arp (1964; BA) and by Pellet *et al.* (1978; HP) which were compiled on the basis of Hα emission to aid in identifying the emission nebulae. To avoid multiplying names, we use the BA appellation whenever possible.

Of the seven SNR candidates reported by Kumar (1976), six were within the areas we photographed, and each of those showed strong [S II] relative to Hα + [N II] when compared to other emission regions of about the same Hα + [N II] surface brightness. Of the remaining 12 SNR candidates of the 19 listed by DDB1, 5 were detected independently by our search (BA 474, BA 449, BA 581, BA 160, and BA 22). We subsequently searched the positions of the remaining seven candidates from DDB1. We found that two were not emission regions, since they appeared on our continuum plates (1.10 and 1.14 from the list of DDB1; 1.14 is incorrectly identified as BA 550). Two of their candidates appeared to be normal H II regions (BA 330 and BA 439). Two more appeared to have slightly enhanced [S II] emission, but were too close to the edge of our fields for us to form a definite opinion (BA 337 and BA 370). One object, 1.3 from DDB1, was too faint to identify on our plates.

Conversely, we have identified a number of objects which have stronger [S II] than average H II regions but which were not listed by DDB1. As discussed below, spectroscopy of two of these objects, BA 212 and BA 100, shows that they do have strong [S II], but other spectroscopic and morphological considerations make these uncertain SNR candidates.

We measured the size of each SNR candidate using a Mann measuring engine and tabulated these sizes in Table 3. Although size was *not* a deliberate selection criterion, no unresolved remnants (1″ = 3 pc) have been detected. This may be partially the result of rapid evolution for small remnants, but it seems more likely to result from seeing, instrumental effects, and saturation of the photographic plates.

Since several independent size estimates are now available for most of these objects (DDB1; BA; HP), we show the observed range of measured sizes and give an adopted diameter for each of the objects in Table 3. In determining the adopted diameters, we have tried to take the resolution, depth, and quality of the separate sets of plate material into account. Also in Table 3, we give the galactocentric distances of each of the objects. These were calculated using the major and minor axis distances given by BA, an assumed inclination to the line of sight of 12°.5 (Simien *et al.* 1978), and an assumed distance of 690 kpc for M31 (Baade and Swope 1963).

b) Spectrophotometry

We have obtained spectrophotometry for all but four of the objects listed in Table 3. For extended objects, we used the 1.3 m telescope at McGraw-Hill Observatory, and for small ones we used the 4 m Mayall telescope at KPNO. A log of these observations is given in Table 4.

The data at McGraw-Hill were obtained with the 2000 channel intensified Reticon spectrometer, an improved version of the photon-counting instrument described by Shectman and Hiltner (1976). Slit sizes were chosen to maximize the flux from the object while retaining enough resolution to separate the [S II] λ6717, λ6731 doublet. Measurements of the background caused by the sky plus the galaxy continuum were made 40″ away from the object every 10 seconds. The accumulated sky scans were subtracted from the object scans; then the object scans were placed on a linear wavelength scale, corrected for extinction using a mean extinction table, and placed on a flux scale through observations of white dwarfs whose energy distributions are known (Oke 1974). The spectra generally covered the range of 4000–7400 Å with a resolution of 10–12 Å. A McGraw-Hill spectrum for BA 490 is shown in Figure 3*a*.

For very small objects, we obtained spectra with the Image Dissector Scanner on the 4 m telescope at KPNO. The data were reduced at KPNO using the standard data reduction programs. The spectral resolution is somewhat poorer than in the McGraw-Hill data, typically near 18 Å (FWHM), and the spectral coverage was essentially the same, except for BA 449. The KPNO system has substantially better blue response, especially shortward of 4000 Å, and much poorer response, particularly longward of 6000 Å, than the McGraw-Hill system. Our reduced 4 m spectra of BA 160 is shown in Figure 3*b*.

These objects are generally very faint, so that the statistical uncertainty in some line strengths is not neg-

TABLE 3

SUMMARY OF M31 SNR CANDIDATES FROM IMAGE-TUBE PHOTOGRAPHY

NAMES(S)	COORDINATES H M S	o ' "	FIELD(S)	GALACTOCENTRIC DISTANCE (KPC)	MEASURED SIZE (PC)	OBSERVED RANGE OF MEASURED SIZES (PC)	ADOPTED DIAMETER (PC)	COMMENTS
BA 55, HP 546	00 40 55	41 10 28	30' & 10' NE	3.6	19 x 20	12 - 20	19	DDB 1.16, Almost Stellar RKF Candidate
BA 521, HP 447	00 40 09	41 09 23	10' NE	4.8	18 x 20	15 - 20	20	DDB 1.13, Almost Stellar RKF Candidate
BA 23, HP 470	00 40 42	41 02 06	10' NE	5.0	39 x 20	20 - 39	32	DDB 1.15, Elongated RKF Candidate
BA 415, HP 327	00 39 03	40 50 16	10' & 30' SW	4.0	40 x 34	20 - 40	35	DDB 1.12, Very Faint RKF Candidate
BA 416, HP 325	00 38 51	40 50 26	10' & 30' SW	5.4	33 x 29	15 - 33	26	DDB 1.11, In Dust Lane RKF Candidate
BA 160, HP 717	00 42 29	41 19 52	30' NE	11.2	17 x 18	17 x 21	18	DDB 1.19, Almost Stellar
BA 22, HP 468	00 41 14	40 57 05	10' NE, 10' SW	11.8	29 x 38	30 - 75	40	DDB 1.18
BA 581, HP 745	00 41 13	41 36 29	30' NE	13.6	21 x 17	17 - 35	25	DDB 1.17
BA 474, HP 118	00 36 40	40 27 50	55' SW	13.9	40 x 35	30 - 40	37	DDB 1.4
BA 490	00 35 04	40 07 00	80' SW	19.3	98 x 96	75 -100	90	DDB 1.1, Knotty Appearance RKF Candidate
BA 380	00 35 53	39 36 27	NOP	22.7	----	-----	--	DDB 1.2, RKF Candidate Not Confirmed
BA 337, HP 82	00 37 09	40 13 15	55' SW	11.7	50 x 44	40 - 60	45	DDB 1.6, Near Edge of Plate
BA 370, HP 21	00 36 48	40 04 44	80' SW	13.9	25 x 23	15 - 25	23	DDB 1.5, Near Edge of Plate
BA 449	00 38 05	40 38 22	30' SW	7.3	18 x 20	14 - 25	19	DDB 1.7, Almost Stellar
BA 439, HP 278	00 38 16	40 45 51	10' & 30' SW	8.5	24 x 18	17 - 24	19	DDB 1.9, H II Region
BA 330, HP 124	00 38 10	40 15 51	55' SW	13.5	32 x 28	20 - 32	30	DDB 1.8, H II Region
BA 212, HP 879	00 42 59	40 39 26	55' NE	10.6	86 x 76	75 -100	80	Circular Appearance
BA 100, HP 625	00 41 29	41 09 58	10' & 30' NE	11.5	42 x 43	33 - 75	45	Diffuse, Irregular Structure

TABLE 4

A. McGraw-Hill 1.3 Meter Observations of M31 SNR Candidates

Object	Date (UT)	Integration Time (s)	Slit Size (″)	Resolution (Å)	Spectral Coverage (Å)
BA 490	1978 Sep 7	4200	2.8 × 40	10	4050–7400
	1978 Sep 9	4800			
BA 416	1978 Sep 8	4200			
	1978 Nov 27	6000	4 × 10	12	4000–7200
	1978 Nov 28	4500			
BA 23	1978 Dec 3	7800			
	1978 Dec 4	4500	4 × 10	12	4500–7000
	1978 Dec 5	3900			
BA 22	1979 Nov 15	6600	2.8 × 10	10	3600–7500
BA 581	1979 Nov 18	3000	4 × 10	12	3800–7500
	1979 Nov 19	2100			
BA 474	1979 Nov 17	5400	4 × 40	12	4200–7400
BA 212	1979 Jan 2	3000	4 × 20	12	3700–7400
BA 100	1980 Jan 21	1800	4 × 10	12	4100–7800
BA 370	1980 Aug 5	3600	4 × 10	12	3600–7400
	1980 Aug 6	4800			

B. KPNO 4 Meter Observations of M31 SNR Candidates

Object	Date (UT)	Integration Time (s)	Slit Size (″)	Resolution (Å)	Spectral Coverage (Å)
BA 521	1978 Sep 1	4400	5.3	15	4000–7500
BA 55	1978 Sep 1	2400	5.3	15	4000–7500
BA 160	1979 Sep 19	3400	5.3	15	3650–7100
BA 449	1979 Sep 18	1600	5.3	5	5850–7150
BA 330	1979 Sep 16	3600	5.3	15	3600–7100
BA 439	1979 Sep 19	4400	5.3	15	3700–7150

ligible. We estimate, for the worst cases, that the uncertainty in relative line strengths is 20% for lines as strong as Hβ. Errors in the absolute flux of Hβ may be somewhat larger.

The results of our spectrophotometry are given in Table 5, where observed line fluxes, $F(\lambda)$, are given on a scale where $F(\mathrm{H}\beta) = 100$. Also listed are reddening corrected line fluxes, $I(\lambda)$, scaled to $\mathrm{H}\beta = 100$. This reddening correction has been performed using the Whitford (1958) reddening law in the form given by Miller and Mathews (1972). We have corrected all of our data assuming a theoretical ratio of $I(\mathrm{H}\alpha)/I(\mathrm{H}\beta) = 3.0$, which is consistent with a large range of shock models (Raymond 1979; Shull and McKee 1979) and with recombination theory (Brocklehurst 1971) within the accuracy of the observations. The observed flux in Hβ and the adopted A_v are also listed in Table 5.

For galactic SNRs, the ratio of Hα to [S II] is smaller than 2.5 (i.e., log (Hα/[S II]) < 0.4; see D'Odorico 1978). In these cases, radio observations are available to confirm the nature of the object, and the optical and radio morphology can be compared with the prototypes (van den Bergh, Marscher, and Terzian 1973). Extending the analysis to LMC remnants shows that, despite differences in interstellar abundances between our Galaxy and the LMC, the same ratio still provides a clear discriminant between SNRs and H II regions.

Beyond this sample, it is difficult to provide independent confirmation that an observed nebula is in fact a SNR. However, the data from DDB2 show that M33 H II regions can be separated from SNRs using the same criterion. In Figure 4 we show the data for M33, along with our own observations of the M31 SNR candidates. The figure shows that nitrogen lines in M31 are generally stronger than in M33: in § III*d* we attribute this to a difference in nitrogen abundance. We find that all but two of the M31 objects lie in the region occupied by SNRs in our Galaxy, the LMC, and M33. Those two are BA 330 and BA 439 which were candidates in the list of DDB1, but which we classified as H II regions from our image-tube plates. The weak [O II] λ3727 and the absence of [O I] λ6300 in these objects also suggest that they are in fact H II regions and not SNRs. In our discussion of SNRs in M31, we omit BA 330 and BA 439.

Two other objects, BA 100 and BA 212, were selected from our image-tube plates, and they fall in the SNR region of Figure 4. However, they are quite unlike galactic SNRs in other respects. BA 100 is a large (42 pc diameter), diffuse emission region which has both emission lines and a blue continuum in its spectrum. This probably indicates the presence of O or B stars in the nebula. BA 212 is an immense (80 pc diameter), circular region which may also have exciting stars nearby. Neither object shows measurable [O I] λ6300, which is generally

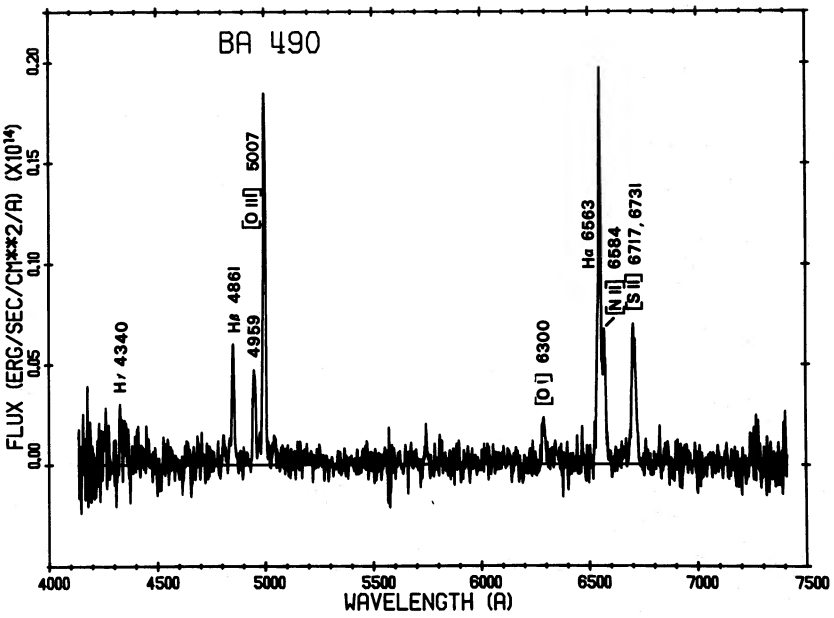

FIG. 3*a*

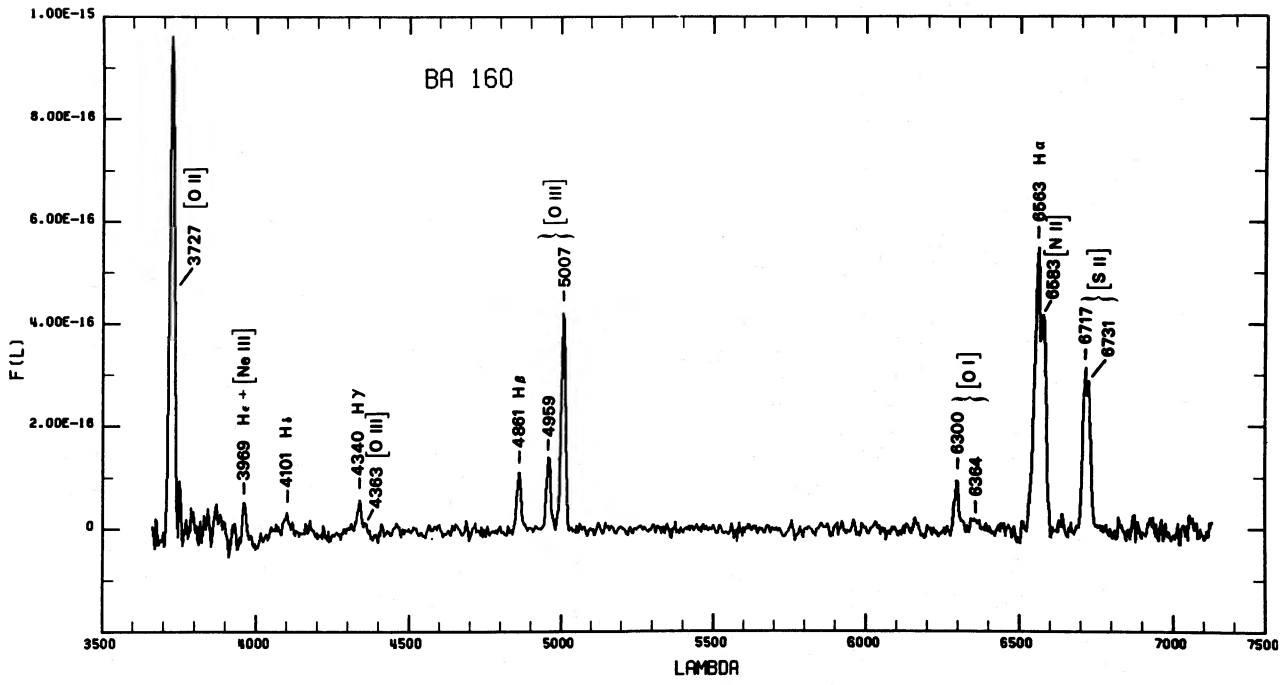

FIG. 3*b*

FIG. 3.—(*a*) McGraw-Hill Reticon spectrum of BA 490. (*b*) KPNO 4 m IIDS spectrum of BA 160.

TABLE 5

OBSERVED FLUXES $F(\lambda)$ AND REDDENING CORRECTED FLUXES $I(\lambda)$ RELATIVE TO $H\beta = 100$

Line I.D.	λ	BA 55 F(λ)	BA 55 I(λ)	BA 521 F(λ)	BA 521 I(λ)	BA 23 F(λ)	BA 23 I(λ)	BA 416 F(λ)	BA 416 I(λ)
[O II]	3727								
[Ne III]	3869								
[Ne III] + Hε	3968								
[S II]	4070	32	38	<25	<27			<55	<70
Hδ	4101	<28	<33	<28	<30			<41	<51
Hγ	4340	55.3	63.6	36.9	38.9			<54	<66
[O III]	4363	32.5	37.3	<25	<26.3			<50	<61
Hβ	4861	100	100	100	100	100	100	100	100
[O III]	4959	144	141	72.8	72.2	21.9:	21.7:	136	132
[O III]	5007	357	345	184	182	102	100	416	399
[N I]	5200	<19	<17	<22	<20	<30	<29	<50	<46.3
[N II]	5755	<11	< 9	<17	<15	<25	<23	<40	<32
He I	5876	26.0	21.3	34.7	31.5	<25	<23	<86	<66
[O I]	6300	77.8	59.5	110	99.8	74.0:	65.5:	148:	104:
[O I]	6363	32.6	24.7	38	34.2	76.0:	66.0:	80.4:	56.3:
[N II]	6548	150	111	128	114	102	87.0	221	146
Hα	6563	407	300	337	300	359	300	455	300
[N II]	6584	452	332	385	343	306	261	664	438
[S II]	6717	256[a]	185	244[a]	216	173	149	336	215
[S II]	6731	256[a]	185	210[a]	186	140	121	282	180
[Ar III]	7136	30:	20.4:	39:	33.5:				
[Ca II]	7291	<32	<22	<50	<43				
[O II] + [Ca II]	7324	47.4	30.8	<50	<43				
F(Hβ)(ergs cm^{-2} s^{-1})		1.23 E-15		4.99 E-16		2.40 E-15		8.44 E-16	
A_V (mag)		0.84		0.32		0.38		1.21	

seen in SNRs, and both show much weaker [O III] λ5007 than the other SNR candidates.

It is possible that one or both of these objects may be a very old SNR with a low shock velocity, but they may also be the result of stellar winds in an OB association. In any event, these two nebulae are basically different from the other 11 SNRs we have observed. While these objects deserve further study to see whether they are related to the giant loops in the LMC (Lasker 1979) or other objects, we have left them out of the interpretation of the SNR spectra in § III.

III. INTERPRETATION

a) Temperature

The most clear-cut way to establish that the nebulae we have selected are, in fact, shock-heated SNRs is to measure the temperature in the [O III] lines. For shock-heated nebulae the ionization is collisional, so the electron temperature in the O^{++} zone should be 25,000 K or more, rather than the 10,000 K typically observed in photoionized nebulae.

Although most of our objects are too faint to allow a good measurement of [O III] λ4363, we have measured this line in four objects. After Osterbrock (1974), we have used the data corrected for reddening from Table 5 to determine the O^{++} temperature. Our best estimates for the four remnants are given in Table 6, which shows T_e in the range of 37,000–65,000 K. Of course, there is a strong bias at work here: we can only measure the electron temperature when it is high. For comparison, Miller (1974) found $39{,}000 < T_e < 49{,}000$ K in three Cygnus Loop filaments, and Fesen and Kirshner (1980) measured T_e near 24,000 K in the galactic remnant IC 443.

The tendency in measuring weak lines is generally to overestimate their strength: in Table 6 we show that the O^{++} temperature is still high, even if we assume that the $I(\lambda 4363)$ values in Table 5 are 50% too large. We believe that the high O^{++} temperatures found in these objects

TABLE 5—*Continued*

Line I.D.	λ	BA 449[b] F(λ)	BA 449[b] I(λ)	BA 160 F(λ)	BA 160 I(λ)	BA 22 F(λ)	BA 22 I(λ)	BA 581 F(λ)	BA 581 I(λ)
[O II]	3727			868	1224				
[Ne III]	3869			46:	63:				
[Ne III] + Hε	3968			67	91.5				
[S II]	4070			<15	<19				
Hδ	4101			29.3:	36.6:				
Hγ	4340			50.2	61.7	50:	62:	37.5:	46.6:
[O III]	4363			25	29.4			24.5:	30.5:
Hβ	4861			100	100	100	100	100	100
[O III]	4959			123	119	88.0	84.8	152	147
[O III]	5007			356	339	308	291	419	399
[N I]	5200			<13	<12	28:	25:	25:	23.3:
[N II]	5755			<20	<16	<25	<20	<30	<24
He I	5876	35.8	—	<17	<13	<40	<29	<30	<24
[O I]	6300	105	—	81	54.7	114	72.0	122	81
[O I]	6363	33.7	—	24.3:	17.5:	45:	29:	20:	13:
[N II]	6548	86.7	—	120	77.4	154	91.4	97.9	61.5
Hα	6563	300[b]	—	468	300	505	300	478	300
[N II]	6584	290	—	363	232	464	274	293	183
[S II]	6717	206	—	225	140	286	164	249	151
[S II]	6731	187	—	209	130	227	130	198	120
[Ar III]	7136	<45				<30	<16	<30	<19
[Ca II]	7291					<25	<13	<20	<12
[O II] + [Ca II]	7324					87:	44:	61:	33:
F(Hβ) (ergs cm^{-2} s^{-1})		2.85 E-15[b]		2.05 E-15		2.20 E-15		2.40 E-15	
A_V (mag)		—		1.24		1.45		1.09	

provide clear evidence that we are dealing with shock-heated nebulae.

b) Density and Energy

We have determined the electron density in the S^+ zone of each of our remnants by measuring the density-sensitive line ratio of [S II] $I(\lambda 6717)/I(\lambda 6731)$ and comparing it to calculations based on the cross sections of Pradhan (1978). In most of our spectra, the peaks of the two lines are reasonably well separated, but the complete lines are not clearly resolved. To measure the line ratios in the 4 m data, we used the relative peak intensities. For the McGraw-Hill data we employed a Gaussian line-fitting program. The second approach is less vulnerable to noise, and the two methods agree when the data have good signal to noise. We believe that all of our [S II] line ratios are reliable, except for the measurement of BA 474 which is considerably affected by noise.

The densities we measure are in the range of 150–730 cm^{-3}, which is comparable to the values found in galactic remnants. Because the temperature in the S^+ zone is likely to be near 10^4 K, it is possible to estimate the pressure in the filaments of the remnant from the [S II] density estimate. Model calculations of cooling shocks by Dopita (1977*a*) show that the pressure just behind the shock can be connected to the observed [S II] density by

$$N_0 V_7^2 = N(\text{S II})/45 , \quad (1)$$

where N_0 is the preshock density in the gas that becomes an optical filament, and V_7 is the shock velocity in units of 10^7 cm s^{-1}.

In the picture of SNRs sketched by McKee and Cowie (1975), the blast wave from the supernova explosion propagates through an inhomogeneous interstellar medium. In dense interstellar clouds, cooling shocks give rise to the optical emission, while in the intercloud region a fast shock heats the gas to temperatures where X-rays are emitted. A rough pressure equilibrium prevails between the two regions, so that an estimate of the pressure in the optical filaments can be used to estimate the energy density in the interior of the entire remnant. According to McKee and Cowie (1975), we can write

$$E_0 = 2 \times 10^{46} (\beta')^{-1} N_0 V_7^2 R(\text{pc})^3 \text{ ergs} , \quad (2)$$

where E_0 is the initial energy in the explosion. Here β' is the ratio of the pressure in the cloud to the pressure in the intercloud medium: it is of order unity.

TABLE 5—*Continued*

Line I.D.	λ	BA 474 F(λ)	BA 474 I(λ)	BA 370 F(λ)	BA 370 I(λ)	BA 490 F(λ)	BA 490 I(λ)	BA 330 F(λ)	BA 330 I(λ)
[O II]	3727			400	431			182	368
[Ne III]	3869							<15	<29
[Ne III] + Hε	3968							<30	<55
[S II]	4070							<15	<24
Hδ	4101			22.0:	23.2:	<33	<35	22:	33:
Hγ	4340			41.2	42.9	30.9	31.7	35.6	49.3
[O III]	4363					20.7:	21.3:		
Hβ	4861	100	100	100	100	100	100	100	100
[O III]	4959	95.0	93.6			89.9	89.5	<20	<18
[O III]	5007	218	213	<30	<29	331	329	<20	<18
[N I]	5200					< 6	< 6		
[N II]	5755					20:	19:		
He I	5876	<33	<29	<22	<21	< 7	< 7		
[O I]	6300	148	124	73.2	67.2	43.2	41.1		
[O I]	6363	54.8	45.3	22.0:	20.3:	11.4	10.8		
[N II]	6548	67.0	54.7	40.2	37.5	38.8	36.7	64.8[a]	29.2
Hα	6563	368	300	328	300	317	300	668[a]	300
[N II]	6584	201	164	122	112	116	110	194[a]	86.5
[S II]	6717	195[a]	157	133	122	118	111	95	40.4
[S II]	6731	188[a]	151	114	104	90.2	85.0	78	33.0
[Ar III]	7136	<30	<24			15.8	14.7	<25	<10
[Ca II]	7291	<60	<47			24:	22:		
[O II] + [Ca II]	7324	<60	<47			35:	32:		
F(Hβ)(ergs cm^{-2} s^{-1})		4.00 E-15		4.10 E-15		8.39 E-15		4.00 E-15	
A_V (mag)		0.56		0.27		0.16		2.20	

The value of E_0 derived from equation (2) is given for each remnant in Table 7. The values found for BA 474 and BA 490 are probably spurious: for BA 474, the [S II] lines are contaminated by noise, and for BA 490 the [S II] ratio is so near the low-density limit that a small observational error can make a large difference in the derived density. The average energy from the nine dependable entries in Table 7 is $\langle E_0 \rangle \approx 3 \times 10^{50}$ ergs. For comparison, the same technique applied to the Cygnus Loop gives about 7×10^{50} ergs.

It can be seen from Figure 5 that the energies estimated from equation (2) tend to increase with the diameters of the remnants. This applies not only to M31 SNRs, but also to those in the LMC (Dopita 1979), our Galaxy (Daltabuit, D'Odorico, and Sabbadin 1976), and M33 (DDB2). We consider several possible reasons for this effect.

First, it is possible that the sizes of the remnants have been underestimated. RCW 86 is a good example of a remnant where only a small region is optically bright (see photograph in van den Bergh, Marscher, and Terzian 1973). Radio and X-ray estimates of remnant sizes are probably more reliable than optical estimates. The lack of small remnants with normal energies could result from the absence of small remnants which are in the radiative phase (with radiating shock waves).

Another possibility is that there is a range of supernova energies, and the remnants enter the radiative phase of evolution at various radii as a result of their energy spread. Remnants are expected to be most prominent optically at the time that they enter the radiative phase. They are not visible before this time because the post-shock temperature is too high for efficient cooling, and they become less prominent after this time because the shock velocity drops approximately as R^{-3}. According to Cox (1972*b*), the critical radius for entering the cooling phase, R_c, depends on supernova energy, E_0, to the $\frac{5}{17}$ power. If E_0 varies by a factor of 10, R_c varies by 2.0. This is in approximate accord with the observations. However, one difficulty with this explanation is that observations of extragalactic supernovae do not seem to be compatible with energies as low as 10^{49} ergs.

There are some additional observations which are not clearly compatible with these two explanations. First, the X-ray observations of Long and Helfand (1979) of remnants in the LMC do not show any trend of E_0 with R, where E_0 is now estimated from the X-ray luminosity. However, their sample of remnants only partially over-

TABLE 5—*Continued*

Line I.D.	λ	BA 439 F(λ)	BA 439 I(λ)	BA 100 F(λ)	BA 100 I(λ)	BA 212 F(λ)	BA 212 I(λ)
[O II]	3727	304	353			380	460
[Ne III]	3869	<20	<23				
[Ne III] + Hε	3968	<21	<23.5				
[S II]	4070	<15	<16				
Hδ	4101	29.2	32.4				
Hγ	4340	41.7	45.1			47.1	52.1
[O III]	4363						
Hβ	4861	100	100	100	100	100	100
[O III]	4959	<14	<14	48.7:	48.5:	<25	<25
[O III]	5007	24.6	24.2	82.2	81.5	<40	<40
[N I]	5200						
[N II]	5755						
He I	5876	14:	12.5:	25:	23:	<18	<15
[O I]	6300	<18	<15	<17	<16	<30	<25
[O I]	6363	< 9	< 8				
[N II]	6548	54.9	46.3	47.2	43.7	38.8	31.3
Hα	6563	356	300	324	300	373	300
[N II]	6584	165	139	142	131	117	93.6
[S II]	6717	36.4	30.3	98.3	90.4	131	103
[S II]	6731	34.3	28.6	80.0	73.5	94.9	74.9
[Ar III]	7136						
[Ca II]	7291						
[O II] + [Ca II]	7324						
$F(H\beta)$ (ergs cm^{-2} s^{-1})		1.84 E-13		1.80 E-14		1.62 E-14	
A_V (mag)		0.47		0.22		0.60	

NOTE.—Colon after number indicates that the line was substantially affected by noise or night sky.
[a] Peaks not resolved, deblending uncertain.
[b] Observed only at high dispersion in the red. Scaled to $F(H\alpha) = 300$.

laps the optical sample of remnants, and their radii are estimated from optical and radio observations. Second, observations of IC 443 show that the pressure estimated from the [S II] lines, which is the basis for the E_0 estimates given here, is nearly an order of magnitude smaller than the pressure estimated from X-ray observations (Fesen and Kirshner 1980).

Dopita (1979) has claimed that the apparent relation between E_0 and R can be explained by the cloudlet evaporation model for SNRs which has been developed by McKee and coworkers (see McKee and Ostriker 1977 and references therein). In this model, thermal evaporation from the shocked cloudlets enhances the density of the intercloud region. The importance of this effect decreases in larger remnants, since the mean density of the intercloud region decreases as a remnant expands. Dopita asserts that this effect mimics a situation where a blast wave is moving down a density gradient. He investigates a special case where the external density drops as R^{-2} and finds that this can reproduce the $E_0 \propto R^{-2.3}$ relation which is found for the LMC remnants (when E_0 is calculated by a method similar to eq. [2]). However, the crucial parameter is the internal pressure profile. Dopita's model requires a steep pressure gradient inside the remnant with $P \propto (r/R)^5$, where r is the distance from the center of the remnant. While McKee and Ostriker do not compute the internal structure in detail, they do note that conduction should tend to give smooth temperature and density profiles, and thus produce a pressure profile with little variation. Without a clear demonstration that the pressure drops steeply behind the shock, Dopita's picture does not provide a natural explanation of the apparent $E_0 - R$ relation, although such a model is not ruled out.

An idea that seems to be capable of explaining the observations is that the [S II] emitting regions are not dominated by the thermal pressure, as is assumed in equation (2), but by magnetic pressure. In this case, the

TABLE 6

TEMPERATURE DETERMINATIONS FOR M31 SNRs

Object	$\frac{I(5007+4959)}{I(4363)}$	T([O III]) (K)	Lower Limit (K)
BA 55	13.0	~65,000	≳29,000
BA 160	15.6	~47,000	≳25,000
BA 490	19.7	~37,000	≳20,000
BA 581	17.9	~38,000	≳20,000

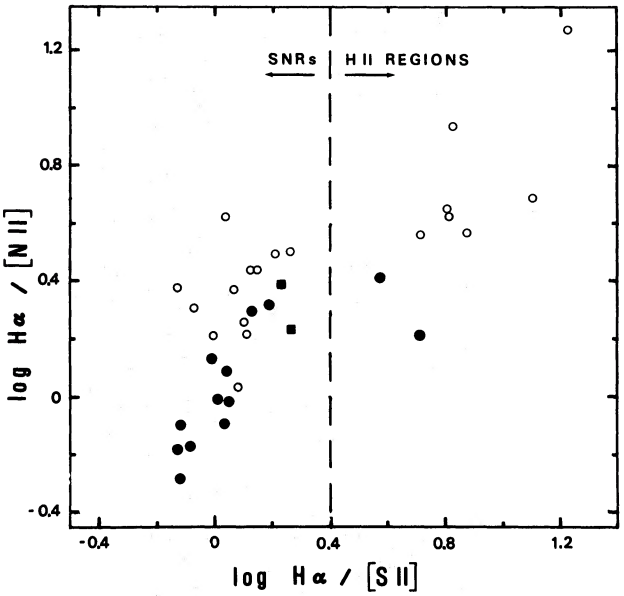

FIG. 4.—Log Hα/[N II] vs. log Hα/[S II] for our M31 observations (*filled circles*) and M33 observations by DDB2 (*open circles*). The dashed vertical line has been found to successfully delineate between SNRs and H II regions in our Galaxy and the Magellanic Clouds. The two squares are BA 100 and BA 212 and are probably not SNRs (see text).

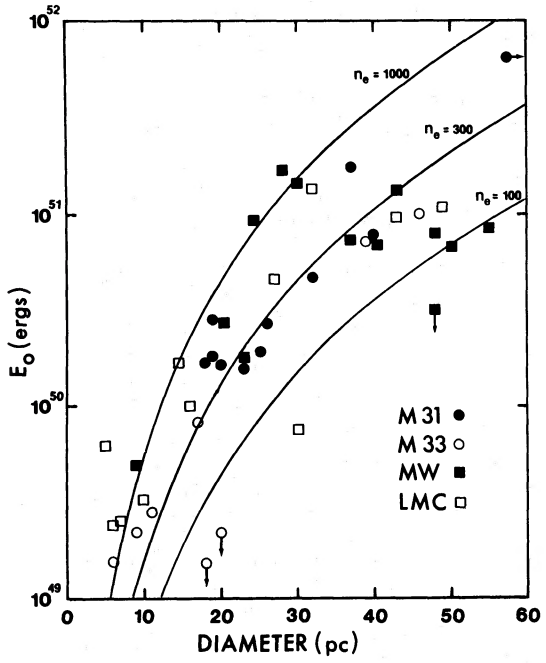

FIG. 5.—Initial energy calculated using eq. (2) vs. diameter for SNRs in M31 (*filled circles*), M33 (*open circles*), the Milky Way Galaxy (*filled squares*), and the LMC (*open squares*). The curves are lines of constant density and are not intended to fit the data. Several of the smaller diameter M33 SNRs have $E_0 < 10^{49}$ ergs and are not shown here. Also, the uppermost M31 point is BA 490, which is plotted at the correct energy but has a diameter of 90 pc.

TABLE 7

DENSITIES AND INITIAL ENERGIES[a] OF M31 SNRs

Object	N(S II) (cm^{-3})	$N_c V_{c7}{}^2$	E_0 (10^{50} ergs)
BA 55	730	16.2	2.78
BA 521	360	8.00	1.61
BA 23	255	5.67	4.65
BA 416	275	6.11	2.69
BA 449	470	10.4	1.79
BA 160	530	11.8	1.73
BA 22	210	4.67	7.47
BA 581	220	4.89	1.91
BA 370	345	7.67	1.56
BA 474	<600	<13.8	<17.6
BA 490	155	3.44	62.7

[a] Assuming $\beta' = 1$.

energies are underestimated by the ratio of thermal pressure to magnetic pressure. In this model, all the supernovae have similar energies and the radiating shock waves are caused by the interaction of the blast wave with clouds. Considering the compression of the magnetic field in the cooling shock wave, the maximum density in the postshock region is given by (McKee and Hollenbach 1980),

$$n_m = 77 \frac{N_0{}^{3/2} V_7}{B_{0\perp -6}} \text{ cm}^{-3} , \quad (3)$$

where N_0 is the cloud density, V_7 is the shock velocity in units of 10^7 cm s^{-1}, and $B_{0\perp -6}$ is the preshock perpendicular magnetic field in units of 10^{-6} gauss. For $N_0 = 10$ cm^{-3}, $V_7 = 1$, and $B_{0\perp -6} = 5$, $n_m = 500$ cm^{-3}, which is in the observed range. Assuming that the interstellar medium has similar properties throughout, N_0 and $B_{0\perp -6}$ are always the same. However, V_7 is expected to be proportional to $R^{-3/2}$, so $n_m \propto R^{-3/2}$ and E_0 (calculated from eq. [2]) $\propto R^{3/2}$. This R dependence of E_0 is weaker than is observed.

Another variant of this idea includes the possibility that the magnetic field is amplified at the shock. By modeling the nonthermal emission from young remnants, Reynolds and Chevalier (1981) concluded that several percent of the postshock energy density goes into an amplified magnetic field. In this case, the maximum density is $n_m \approx 33 n_0$, independent of the shock velocity. For $N_0 = 10$ cm^{-3}, $n_m = 330$ cm^{-3}, which is in the observed range. E_0 (calculated from eq. [2]) is proportional to R^3, which is close to the observed relation.

The various models for the $E_0 - R$ relation make different predictions for the dependence of the shock velocity, v_s, on R. The first model does not make a specific prediction, but the fact that the pressures are similar in the various remnants implies that the shock velocities are similar. In the second model, v_s is not expected to depend strongly on R because cooling always becomes important at about the same temperature and shock velocity. Using the relations in Cox (1972*b*) and assuming that the shock velocity is proportional to the cooling radius divided by the cooling time, we find $v_s \propto R^{0.2}$. Finally, in the magnetic model, the postshock pressure is simply given

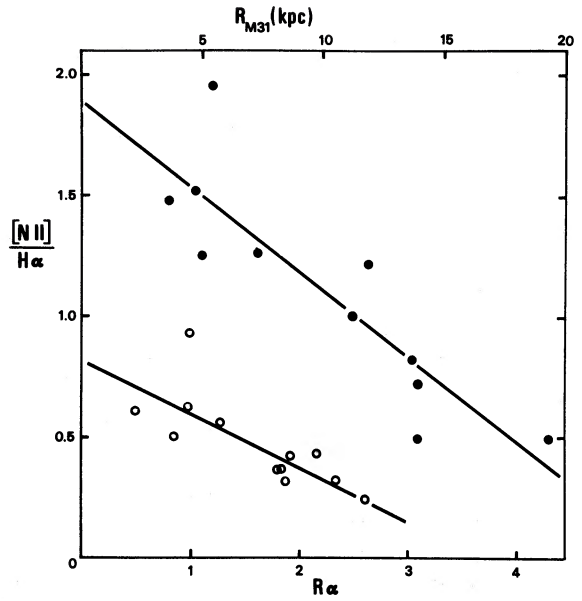

FIG. 6a

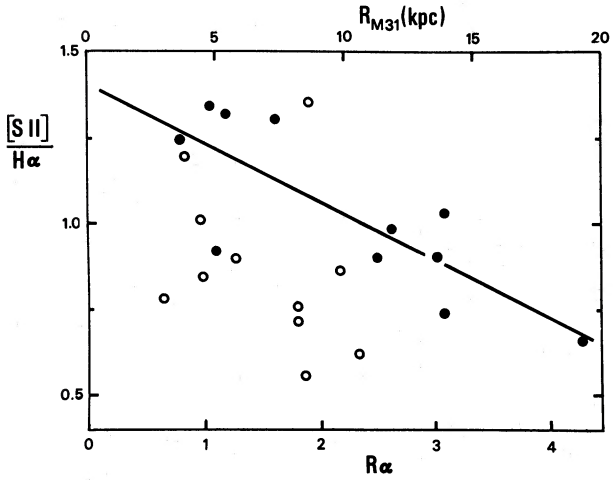

FIG. 6b

FIG. 6.—(*a*) [N II] λλ6548, 6584 strength relative to Hα vs. galactic radius for M31 SNRs (*filled circles*) and M33 SNRs (*open circles*). The two galaxies have been scaled relative to one another using their photometric disk scale lengths (α^{-1}) from Freeman (1970). (*b*) Same as (*a*), but for the [S II] λλ6717, 6731 line strength relative to Hα. (*c*) Same as (*a*) and (*b*) except the ordinate is the [N II] λλ6548, 6584 intensity relative to [S II] λλ6717, 6731.

by the total energy divided by the volume, so the shock velocity is expected to drop as $R^{-1.5}$. It is clear that velocity measurements could be helpful in distinguishing between the various models. For the LMC remnants, Dopita (1979) obtains an "expansion" velocity determined from the maximum velocity in the [O II] line profile. He finds that, after a slight intial rise, this velocity drops approximately as $R^{-0.45}$. This may suggest that more than one effect is important in determining the remnant radii, energies, and velocities. However, it is not clear that the expansion velocity is the same as the typical shock velocity. Other methods to determine velocities,

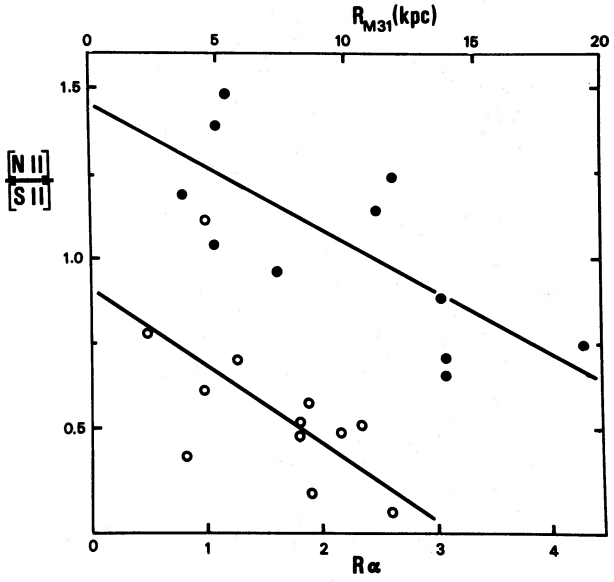

FIG. 6c

such as from relative line strengths, will be useful. Also, X-ray observations should be useful in clarifying the problem of energetics.

c) *An Abundance Gradient?*

We would like to compare our measured line strengths for N, O, S, and H to estimate chemical abundances in the interstellar gas of M31 by comparing our results with the predictions of models for cooling shock waves. All of the remnants that we have observed are large enough that any freshly synthesized material should be dominated by the ambient gas swept up by the shock. Recent numerical work by Dopita (1977*a*), Raymond (1979), and Shull and McKee (1979, hereafter SM) has improved on the early work by Cox (1972*a*, *b*). While the available range of models is not adequate to fit a particular observation uniquely, the models do provide an important guide to interpretation of spectra.

For example, the models show that the strength of [O III] relative to Hβ is a sensitive function of the shock velocity. Hence, [O III]/Hβ may be a useful ratio to establish a limit on the shock velocity, but without other knowledge of the velocity and observations of O° and O^+, it is unreasonable to derive information on the oxygen abundance from this ratio. Since in most cases we lack [O II] λ3727 observations, we will not attempt to derive the O abundance here.

The case of nitrogen is much more favorable: the ratio [N II] λ6548 + λ6583/Hα is much less sensitive to shock velocity, changing less than a factor of 2 over the velocity range of interest. The [N II]/Hα line ratio depends linearly on the N/H abundance ratio, a result that has been previously employed in abundance analyses of SNRs (D'Odorico and Sabbadin 1976*a*; DDB2). In Figure 6*a*, we plot [N II]/Hα against galactocentric distance, which shows that the [N II]/Hα ratio decreases by a factor of 4 from the innermost SNR at $\lesssim 4$ kpc to the outermost at

almost 20 kpc. We suggest that the nitrogen abundance is about 4 times higher in the inner region than at 20 kpc.

It is unfortunate that the measured variation in [N II] strength depends to a considerable extent on the outermost point (BA 490), which is also the largest SNR in the sample. If some effect related to the evolution of remnants affects the [N II]/Hα ratio, this point might be altered the most (e.g., D'Odorico and Sabbadin 1976*b*; Dopita 1977*b*). However, even if BA 490 were (unfairly) ignored, the trend in [N II]/Hα would still be established by the remnants near 11–14 kpc whose radii vary from 18–40 pc.

It is conceivable that the observed nitrogen gradient might be the result of different absorption of nitrogen on interstellar grains across the galaxy. We consider this to be unlikely because nitrogen is one of the least depleted elements in the interstellar mix (Spitzer and Jenkins 1975). Furthermore, there is some evidence that interstellar grains are destroyed by their passage through a supernova shock (Fesen and Kirshner 1980). In that event, even if some nitrogen is absorbed onto grains, we would observe the total nitrogen abundance in the gas phase well downstream from the shock.

In Figure 6*b*, we show the gradient in [S II] line strength. Although de-excitation could possibly confuse the interpretation of the [S II] lines, our $I(\lambda 6717)/I(\lambda 6731)$ measures show that this effect cannot be dominant. The results could be interpreted as a gradient in S abundance, but better information on each remnant's shock would be very helpful in reducing the uncertainty in S/H. The most useful way to examine the [S II] lines is to compare them with the [N II] lines that are formed in about the same region of a cooling shock, because the ionization potentials are similar. In Figure 6*c*, we show that [N II]/[S II] also decreases with increasing galactic radius, which may indicate that N/S is higher in the inner regions. It seems premature to interpret these trends in terms of nucleosynthesis processes.

The more detailed observations of M33 SNRs by DDB2 have allowed them to interpret their line ratios as abundance gradients of N/O and N/S in that galaxy. While our present data in M31 are not adequate to derive detailed abundance estimates, it is instructive to compare the line ratios of the M33 SNRs with our data for M31. In Figures 6*a*, *b*, and *c*, we also show the M33 observations on the same vertical scale, but with abscissae scaled using the photometric scale lengths of the galactic disks as given by Freeman (1970). As the figures show, the [N II]/Hα ratios for M31 and M33 have very similar variations with radius. Since the M33 observations have already been successfully interpreted as an abundance gradient, it seems likely that the same interpretation will hold for M31. The [S II]/Hα ratio for M33 does not show a clear trend with galactic radius: this is in conflict with our findings for M31. Dopita's (1977*a*) models show that larger oxygen or sulfur abundances tend to decrease the strength of the [N II] lines. Hence, if a sulfur or oxygen gradient is present in M31, then the observed [N II] line intensity gradient requires an even stronger increase in the nitrogen abundance toward the center of M31.

Figures 4 and 6*a* and *c* also show that [N II]/Hα averages about 2.6 times larger in M31 than in the M33 SNRs. Since Dopita's models show that the strength of the [N II] lines (other things being equal) are directly related to the nitrogen abundance, a higher overall nitrogen abundance in M31 appears to be indicated. Furthermore, we can use the observations of galactic SNRs by Daltabuit, D'Odorico, and Sabbadin (1976) to establish a local average value of [N II]/Hα in SNRs, and use the LMC SNR observations of Dopita, Mathewson, and Ford (1977) to obtain an average value of this ratio for the LMC for comparison. Taking the local SNRs as unity for [N II]/Hα, we find that the LMC remnants have [N II] 0.37 times as strong, the M33 remnants are half as strong, and in M31 [N II] is 1.3 times as strong as in our Galaxy. This order from high to low N abundance is what one might expect for these four galaxies: M33 and the LMC are late-type galaxies with high gas content, while M31 and our Galaxy are intermediate-type spirals with moderate gas content. Presumably, M31 and our Galaxy have transformed more of their gas into stars and some of it has been returned to the interstellar gas as nitrogen.

IV. OBSERVATIONS AT OTHER WAVELENGTHS

a) Radio

Radio observations of M31 have lacked the sensitivity and spatial resolution needed to detect SNRs of the kind discussed here. For instance, the 5C 3 survey of Pooley (1969) observed the region in and around M31 at two frequencies and identified over 200 discrete sources, yet only a handful of these were thought to be associated with the galaxy. This has been reiterated by a number of other investigators (van der Kruit 1972; van der Kruit and Katgert 1972; Parkes and Penston 1973; Spencer and Burke 1975). While six sources were found to be near enough to emission regions that they might be associated, only 5C 3.98 has a nonthermal spectral index. The emission regions near this source (BA 384–86) do not appear to have strong [S II] emission on our image-tube plates and, hence, this is probably a chance alignment with a background source. More recent work (Berkhuijsen and Wielebinski 1974) has still not had sufficient resolution and sensitivity to unambiguously detect M31 SNRs. We note in passing that any young, radio bright SNRs comparable in strength to Cas A or the Crab Nebula should have been detected even by these early surveys.

Currently, a comprehensive high resolution multifrequency radio survey of M31 is in progress at Leiden using the Westerbork interferometer (van der Laan 1979). Using the estimated detection limit of 1 mJy at 21 cm and assuming a Σ-D relation from Clark and Caswell (1976), we estimate that SNRs with $D \lesssim 30$ pc should be detected in this survey. This would include eight of the objects listed in Table 3 and might also turn up additional SNRs which were missed by us due to their faintness or small angular size. In Table 8, we show the radio flux we would expect at 408 MHz, assuming the Σ-D relation, and extrapolate this to 21 cm assuming $\alpha = +0.7 (S_\nu \sim \nu^{-\alpha})$.

b) X-Ray

A number of galactic SNRs are strong thermal X-ray sources, and extrapolating these observations to the

TABLE 8

RADIO AND X-RAY PREDICTIONS FOR M31 SNRs

Object	S(408 MHz)[a] (mJy)	S(1420 MHz)[b] (mJy)	L_x/n_0^2 (ergs s^{-1} cm^{-6})
BA 23	5.5	2.3	1.2×10^{37}
BA 521	8.3	3.5	3.0×10^{36}
BA 55	8.8	3.7	2.6×10^{36}
BA 416	6.4	2.7	6.6×10^{36}
BA 449	8.8	3.7	2.6×10^{36}
BA 160	9.3	3.9	2.2×10^{36}
BA 22	0.9	0.4	2.4×10^{37}
BA 581	6.7	2.8	5.9×10^{36}
BA 474	1.7	0.7	1.9×10^{37}

[a] Using Clark and Caswell's (1976) Σ-D relation.
[b] Calculated assuming $S \propto \nu^{-0.7}$.

distance of M31 indicates that some of the M31 SNRs might be observable. Winkler (1978) shows that the X-ray luminosity of an adiabatically expanding SNR can be expressed

$$L(\Delta E) \approx 3.75 \times 10^{55} n_0^2 D^3 P(\Delta E, T) \text{ ergs s}^{-1}, \quad (4)$$

where D is the diameter in pc, n_0 is the ambient density of the surrounding interstellar medium, and $P(\Delta E, T)$ is the X-ray emissivity for the energy band of interest. This relation is approximately correct up to $D \approx 40$ pc, after which the energy peak shifts into the ultraviolet. Using this formula and an emissivity of $P(\Delta E, T) \sim 10^{-23}$ (Gorenstein and Tucker 1976), we can estimate the X-ray luminosity we would expect from each of our SNRs. We list the results of these calculations in Table 8, parameterized to a value of $n_0 = 1$ cm^{-3}. While the ambient densities of each of our SNRs are not known *a priori*, values of $n_0 \approx 1$–3 cm^{-3} would place many of our SNRs above the *HEAO B* detection limit of 9×10^{36} ergs s^{-1} (van Speybroeck *et al.* 1979).

Van Speybroeck *et al.* (1979) have observed the central and NE regions of M31 using the HRI and IPC aboard the *Einstein* X-ray Observatory (*HEAO B*) and have detected 69 sources. The positions of these sources have kindly been made available to us (van Speybroeck 1979), and we have found apparent coincidences between two of the HRI sources and two of the SNRs, BA 23 and BA 521. The observed L_x (0.5–4.5 keV) $\sim 2.2 \times 10^{37}$ ergs s^{-1} for BA 521 implies an ambient density of $n_0 \sim 2.7$ cm^{-3} for the surrounding region, while for BA 23 we have $L_x \sim 1.4 \times 10^{37}$ ergs, implying an $n_0 \sim 1.1$ cm^{-3}. None of the other SNR candidates in the observed regions has been detected.

It is interesting to compare these results to the LMC X-ray observations of Long and Helfand (1979). Their observations for 12 SNRs appear to show an empirical relation between L_x and diameter, with L_x decreasing steeply as a function of size: this is in the opposite sense from equation (4). The two M31 SNRs with observed X-ray emission lie about an order of magnitude above the empirical relation, but the significance of this is uncertain. This is because there is considerable scatter in the empirical relation and some of the LMC remnant diameters are poorly determined. Also, none of the LMC remnants used have diameters in the range 18–30 pc; this is crucial for determining the shape of the relation.

In a forthcoming paper, we will report on additional spectra of emission regions in M31, including better blue spectra of some of the SNRs and spectra of a number of H II regions. The SNR spectra will allow us to estimate abundances which we will compare to the abundances found from analysis of the H II region spectra.

We would like to thank Vera Rubin for helpful discussion and for supplying prints of Baade's original red plates of M31. We also thank Peter Pesch and Case Western Reserve University for the use of their blink comparator machine for the plate search. We are grateful to Sandro D'Odorico who kindly provided us with a copy of DDB1 in advance of publication. The 144 mm ITT image tube was loaned to McGraw-Hill Observatory by KPNO. W. P. B. wishes to thank W. A. Hiltner and the Astronomy Department at the University of Michigan for support while this work was done. This work has also been supported by NSF grant AST 77-17600 and by the Alfred P. Sloan Foundation.

REFERENCES

Baade, W., and Arp, H. 1964, *Ap. J.*, **139**, 1027 (BA).
Baade, W., and Swope, H. H. 1963, *Ap. J.*, **68**, 435.
Berkhuijsen, E. M., and Wielebinski, R. 1974, *Astr. Ap.*, **34**, 173.
Blair, W. P., Kirshner, R. P., Gull, T. R., Sawyer, D. L., and Parker, R. A. R. 1980, *Ap. J.*, **242**, 592.
Brocklehurst, M. 1971, *M.N.R.A.S.*, **153**, 471.
Clark, D. H., and Caswell, J. L. 1976, *M.N.R.A.S.*, **174**, 267.
Cox, D. P. 1972*a*, *Ap. J.*, **178**, 143.
———. 1972*b*, *Ap. J.*, **178**, 159.
Daltabuit, E., D'Odorico, S., and Sabbadin, F. 1976, *Astr. Ap.*, **52**, 93.
Danziger, I. J., Murdin, P. G., Clark, D. H., and D'Odorico, S. 1979, *M.N.R.A.S.*, **186**, 555.
D'Odorico, S. 1978, *Mem. Soc. Astr. Italiana*, **49**, 485.
D'Odorico, S., Benvenuti, P., and Sabbadin, F. 1978, *Astr. Ap.*, **63**, 63.
D'Odorico, S., Dopita, M. A., and Benvenuti, P. 1980, *Astr. Ap. Suppl.*, **40**, 67 (DDB1).
D'Odorico, S., and Sabbadin, F. 1976*a*, *Astr. Ap.*, **50**, 315.
———. 1976*b*, *Astr. Ap.*, **53**, 443.
Dopita, M. A. 1977*a*, *Ap. J. Suppl.*, **33**, 437.
———. 1977*b*, *Astr. Ap.*, **56**, 303.
———. 1979, *Ap. J. Suppl.*, **40**, 455.
Dopita, M. A., D'Odorico, S., and Benvenuti, P. 1980, *Ap. J.*, **236**, 628 (DDB2).
Dopita, M. A., Mathewson, D. S., and Ford, V. L. 1977, *Ap. J.*, **214**, 179.
Fesen, R. A., and Kirshner, R. P. 1980, *Ap. J.*, **242**, 1023.
Freeman, K. C. 1970, *Ap. J.*, **160**, 811.
Gorenstein, P., and Tucker, W. H. 1976, *Ann. Rev. Astr. Ap.*, **14**, 373.
Goss, W. M., Ekers, R. D., Danziger, I. J., and Israel, F. P. 1980, *M.N.R.A.S.*, **193**, 901.
Israel, F. P., and van der Kruit, P. C. 1974, *Astr. Ap.*, **32**, 363.
Kirshner, R. P., and Winkler, P. F. 1979, *Ap. J.*, **227**, 853.
Kumar, C. K. 1976, *Pub. A.S.P.*, **88**, 323.
Lasker, B. M. 1979, *Pub. A.S.P.*, **91**, 153.
Long, K. S., and Helfand, D. J. 1979, *Ap. J. (Letters)*, **234**, L77.
Mathewson, D. S., and Clarke, J. N. 1972, *Ap. J. (Letters)*, **178**, L105.
———. 1973*a*, *Ap. J.*, **180**, 725.

———. 1973*b*, *Ap. J.*, **182**, 697.
McKee, C. F., and Cowie, L. L. 1975, *Ap. J.*, **195**, 715.
McKee, C. F., and Hollenbach, D. 1980, *Ann. Rev. Astr. Ap.*, **18**, 219.
McKee, C. F., and Ostriker, J. P. 1977, *Ap. J.*, **218**, 148.
Miller, J. S. 1974, *Ap. J.*, **189**, 239.
Miller, J. S., and Mathews, W. G. 1972, *Ap. J.*, **172**, 593.
Oke, J. B. 1974, *Ap. J. Suppl.*, **27**, 21.
Osterbrock, D. E. 1974, *Astrophysics of Gaseous Nebulae* (San Francisco: Freeman).
Parker, R. A. R., Gull, T. R., and Kirshner, R. P. 1979, *An Emission-Line Survey of the Milky Way* (NASA SP-434).
Parkes, A. G., and Penston, M. V. 1973, *M.N.R.A.S.*, **162**, 117.
Pellet, A., Astier, N., Viale, A., Courtes, G., Maucherat, A., Monnet, G., and Simien, F. 1978, *Astr. Ap. Suppl.*, **31**, 439 (HP).
Pooley, G. G. 1969, *M.N.R.A.S.*, **144**, 101.
Pradhan, A. K. 1978, *M.N.R.A.S.*, **183**, 89P.
Raymond, J. C. 1979, *Ap. J. Suppl.*, **39**, 1.
Reynolds, S. P., and Chevalier, R. A. 1981, *Ap. J.*, **245**, 912.
Rubin, V. C., Kumar, C. K., and Ford, W. K. 1972, *Ap. J.*, **177**, 31 (RKF).
Sabbadin, F. 1978, *Pub. A.S.P.*, **90**, 563.
Sabbadin, F., and Bianchini, A. 1979, *Pub. A.S.P.*, **91**, 62.
Shectman, S. A., and Hiltner, W. A. 1976, *Pub. A.S.P.*, **88**, 960.
Shull, J. M., and McKee, C. F. 1979, *Ap. J.*, **227**, 131 (SM).
Simien, F., Athanassoula, E., Pellet, A., Monnet, G., Maucherat, A., and Courtes, G. 1978, *Astr. Ap.*, **67**, 73.
Spencer, J. H., and Burke, B. F. 1975, *Ap. J.*, **199**, 611.
Spitzer, L., Jr., and Jenkins, E. B. 1975, *Ann. Rev. Astr. Ap.*, **13**, 133.
van den Bergh, S. 1978, *Ap. J. Suppl.*, **38**, 119.
van den Bergh, S., Marscher, A. P., and Terzian, Y. 1973, *Ap. J. Suppl.*, **26**, 19.
van der Kruit, P. C. 1972, *Ap. Letters*, **11**, 173.
van der Kruit, P. C., and Katgert, P. 1972, *Ap. Letters*, **11**, 181.
van der Laan, H. 1979, private communication.
van Speybroeck, L. 1979, private communication.
van Speybroeck, L., Epstein, A., Forman, W., Giacconi, R., Jones, C., Liller, W., and Smarr, L. 1979, *Ap. J. (Letters)*, **234**, L45.
Whitford, A. E. 1958, *A.J.*, **63**, 201.
Winkler, P. F. 1978, *Mem. Soc. Astr. Italiana*, **49**, 599.

WILLIAM P. BLAIR and ROBERT P. KIRSHNER: Department of Astronomy, University of Michigan, Dennison Building, Ann Arbor, MI 48109

ROGER A. CHEVALIER: Department of Astronomy, University of Virginia, P.O. Box 3818, Charlottesville, VA 22903

PLATE 28

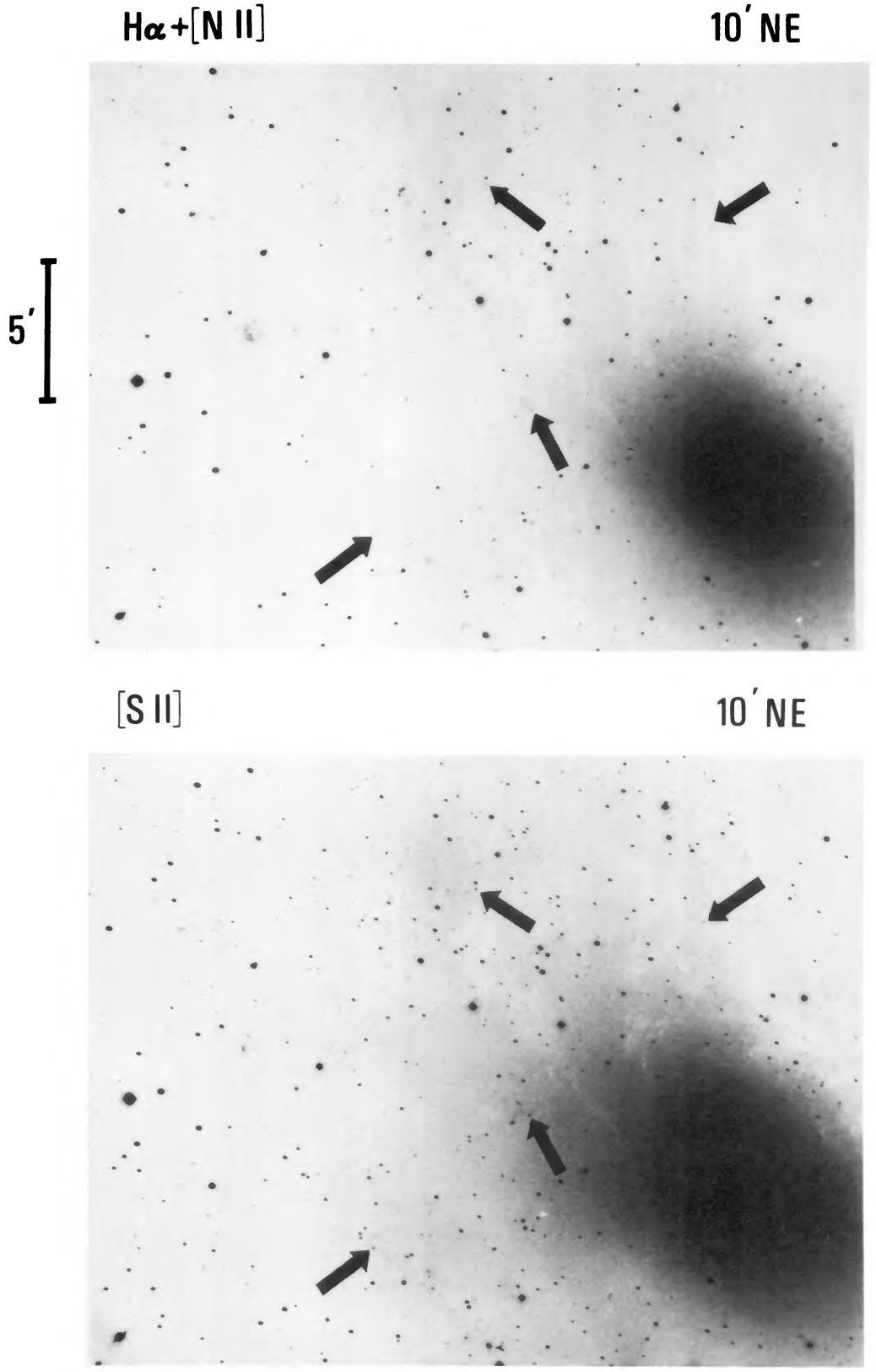

FIG. 2.—Portions of the Hα + [N II] and [S II] photographs centered 10′ NE of the galaxy nucleus. Four of the SNRs are marked with arrows.

BLAIR *et al.* (*see* page 881)